IEEE Photonics Journal
An IEEE Photonics Society Publication

Open Access

A Fast Image Segmentation Algorithm Based on Saliency Map and Neutrosophic Set Theory

Volume 12, Number 5, October 2020

Sensen Song
Zhenhong Jia
Jie Yang
Nikola K. Kasabov, ***Fellow, IEEE***

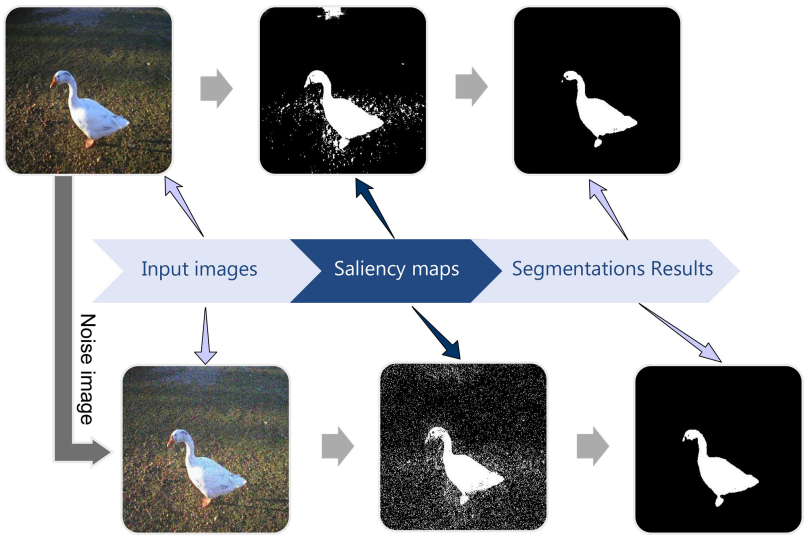

DOI: 10.1109/JPHOT.2020.3026973

IEEE photonics SOCIETY

IEEE

A Fast Image Segmentation Algorithm Based on Saliency Map and Neutrosophic Set Theory

Sensen Song,[1] **Zhenhong Jia**,[1] **Jie Yang**,[2] **and Nikola K. Kasabov**,[3,4] ***Fellow, IEEE***

[1]College of Information Science and Engineering, Xinjiang University, Key Laboratory of Signal Detection and Processing, Xinjiang Uygur Autonomous Region, Xinjiang University, Ürümqi 830046, China
[2]Institute of Image Processing and Pattern Recognition, Shanghai Jiao Tong University, Shanghai 200400, China
[3]School of Engineering, Computing and Mathematical Sciences, Auckland University of Technology, Auckland 1020, New Zealand
[4]Intelligent Systems Research Center, Ulster University, Magee campus BT48 7JL, U.K.

DOI:10.1109/JPHOT.2020.3026973

Manuscript received March 11, 2020; revised September 18, 2020; accepted September 22, 2020. Date of publication September 28, 2020; date of current version October 16, 2020. This work was supported in part by the National Science Foundation of China under Grants 61665012 and U1803261, in part by the International Science and Technology Cooperation Project of the Ministry of Education of the People's Republic of China under Grant DICE 2016–2196, and in part by Natural Science Foundation of Xinjiang under Grant 2015211C288. Corresponding author: Zhenhong Jia (e-mail:jzhh@xju.edu.cn)..

Abstract: Due to more or less deviations in the imaging system, there will be noise in the image, which makes the image segmentation inaccurate. To divide a natural image into a more accurate binary image, the target and background of the image are effectively separated to achieve a more effective segmentation result. Therefore, this paper proposes an image segmentation algorithm combining a saliency map and neutrosophic set (NS) theory. First, to overcome the problem of weak edges in the image, we highlight the details and use the guided filter to filter the various channels of the natural image. Then, the initial saliency map is generated. After the weighted superposition of the initial saliency map, the local entropy map and the gray scale map, the final saliency map can be generated using the nonlinear function, and it can effectively highlight the foreground information of the image. Second, the saliency map is transformed to the NS domain and interpreted by three subsets: true (T), indeterminate (I), and false (F). According to NS theory, the indeterminacy is reduced, and the segmentation results are finally obtained by using the method of threshold. Various experiments were done and compared with other state-of-the-art approaches. These experiments demonstrate the effect of the proposed work, which is fast and effective for de-noising.

Index Terms: Imaging system, image segmentation, neutrosophic set theory, saliency map, the method of threshold.

1. Introduction

For an image, we are only interested in some areas of the image that represent the target to be segmented, while most of the remaining areas of interest can be considered as background. The

salient region is the most interesting and expressive area in the image, and it is also the target of segmentation [1].

First, the saliency map methods are categorized into two classes by defining the features of local or global pixels or regions [2]. One considers the local features [3]–[5], and the other considers the global integrity [6]–[9]. With the continuous emergence of new methods, a method that fuses local features and global integrity has been repeatedly proposed [2], [7], [10], and it can be classified into three categories. In the first category, the differences between pixels (or blocks) and their adjacent pixels (or blocks), differences such as color, brightness, contrast and texture, are calculated. Then, the rich areas can be displayed by using these low-level visual features. The areas with large differences and the details outside the target will be highlighted. Obviously, we do not want all details, which makes the subsequent segmentation appear loose. In the second category, the global optimization is achieved by combining statistical theory, graph theory, hierarchical structuring, spatial domain transformation and other methods. However, the details in the target are not often ignored, which will subsequently lead to over-segmentation. In the third category, the effect of the saliency map will be improved by combining the theoretical advantages of the previous two categories. However, there are still some problems when the objective does not have the same color, gray value, texture and/or set of different regions, which leads to the indeterminacy of the objective. Regardless of the saliency map algorithm, it is urgent to solve the problem of how to accurately capture the target. Therefore, we propose an algorithm combining the local entropy of images with the guidance filtering algorithm based on the L$*$a$*$b space [11], [12] to reduce the impact of previous problems and facilitate the subsequent segmentation. There are many methods of segmentation with a saliency map [13]–[15], such as the clustering algorithm, the level set algorithm, the graph theory algorithm and the deep learning algorithm. The results of these algorithms are directly related to the results of the saliency maps.

In recent years, many saliency detection algorithms have been proposed, and significant progress has been made. For most of the saliency detection algorithms, low-level features, such as color, texture, and contrast, are widely used to describe images. In previous work, the multi-scale and center-surrounding differences were calculated to detect the visual attention area [3]. Another study considered the global information of images by calculating the scale and spatial information of different color attributes [16]. According to the spatial variance information of images, the research detected the highlighted objects based on the assumption that the highlighted objects usually have compact spatial structures [17]. Increasingly, more saliency detection algorithms choose image boundaries as background seeds and detect salient regions by calculating the differences between each region and the background seeds [18]–[20]. Meanwhile, the methods based on deep learning have been developing rapidly in recent years. A novel computational saliency model, i.e., the deep spatial contextual long-term recurrent convolutional network, can predict where people look in natural scenes [21]. Wang *et al.* [22] constructed two kinds of deep convolution neural networks, namely, the local estimation depth network and the global search depth network, with low-level features, such as color and geometric information. In other words, low-level features still play a crucial role in the development of a saliency detection framework for deep learning. However, in most of the cases, the problem is that we need fast saliency detection, and deep learning obviously does not have sufficiently high efficiency. Therefore, unsupervised saliency algorithms are still an important direction for our research.

The neutrosophic set was proposed by Florentin Smarandache as a new branch of philosophy dealing with the origin, nature and scope of neutralities and their interactions with different ideational spectra [23]. The NS algorithm has great advantages in dealing with indeterminacy compared to other methods. Meanwhile, it also has good performance in the field of denoising. NS theory in image segmentation processing [24]–[31] was mainly used for pre-processing images, converting images to the NS domain, and filtering out indeterminacy. However, this paper adopts the method of the saliency map with the NS, which is applied for further processing the saliency map, judging the target, and filtering out the indeterminacy. Finally, the image threshold segmentation method is used for object segmentation.

Image segmentation is used to divide a given image into multiple non-overlapping areas, which is a key technology for subsequent image analysis. NS theory provides a new method to solve the problem of uncertainty, a method which has been used in image processing and has achieved good results. Guo and Cheng [24] proposed an image segmentation algorithm based on NS theory. The image is transformed to the NS domain, which is represented by three membership sets: T, I, and F. In addition, the image entropy is used to characterize its indeterminacy, and two operations, the α-mean and β-enhancement operations, are proposed to reduce the NS indeterminacy. Finally, image segmentation is performed using the γ-means clustering method. Study [28] came up with an image segmentation algorithm combining NS theory with level set theory, which employs a newly defined filter to reduce the image indeterminacy in the NS domain and applies the level set algorithm to automatically extract the boundaries of the objects. An image segmentation algorithm based on neutrosophic similar clustering, and defined cluster similarity functions, which is used for cluster analysis to segment the image, in the NS domain, was also proposed [29]. The main idea in [30] is c-mean clustering and the indeterminacy filter. The indeterminacy filter was employed twice. The first time, the indeterminacy was filtered out through the indeterminacy value of NS domain images and spatial neighborhood information. The indeterminacy filter was then used again after the image c-mean clustering. In another paper [31], the indeterminacy filter was also applied to reduce the indeterminacy of an image through the indeterminacy values and the neighborhood features, and then the image was segmented using mean shift clustering, where the bandwidth was determined by the indeterminacy of the image.

In the saliency map, there is a problem that the useless image details are highlighted, which drowns out useful information, and under-segmentation subsequently occurs. When the indeterminacy is removed in the NS domain, the useful information will be removed, which will lead to over-segmentation. Therefore, the NS theory is applied to remove the indeterminacy factors in the saliency map to overcome the shortcomings of the saliency map and NS theory.

2. Proposed Methods

In this section, a fast image segmentation algorithm based on the saliency map and neutrosophic set model (SMNS) will be introduced in detail, including the construction of the saliency map and a brief description of NS theory. First, the flow chart of the proposed algorithm is shown in Fig. 1. It provides readers with a preliminary understanding of the SMNS model.

As shown in Fig. 1, first, the local entropy map *G1*, the gray scale map *G2*, and the guided filtered saliency map *G3* in the L$*$a$*$b space are respectively calculated. *G1* retains rich details in the image. *G2* mainly compensates for the gray values in *G1* and *G3*. The edges of *G3* are highlighted with color and brightness. Second, the weighted stacking of *G1*, *G2* and *G3* are applied to enhance the object details. Inspired by image enhancement, a saliency map is obtained from the superimposed image using a nonlinear function. Finally, we convert the saliency map into the NS domain, filter out the indeterminacy, and use the threshold value for binary segmentation to get the final segmentation result.

2.1 Construction of the Saliency Map

The main framework of the saliency map has been introduced in the previous algorithm flow chart. We mainly explain the saliency map from three aspects: the local entropy map of the image, the guided filtering that generates a preliminary saliency map, and the nonlinear functional transformation.

2.1.1 Local Entropy Map of the Image

Usually, entropy is used as a standard to measure the quantification of information and to describe the uncertainty of information sources. In image processing, information entropy is employed to evaluate the richness of the details of an image. Generally, the higher the entropy of an image

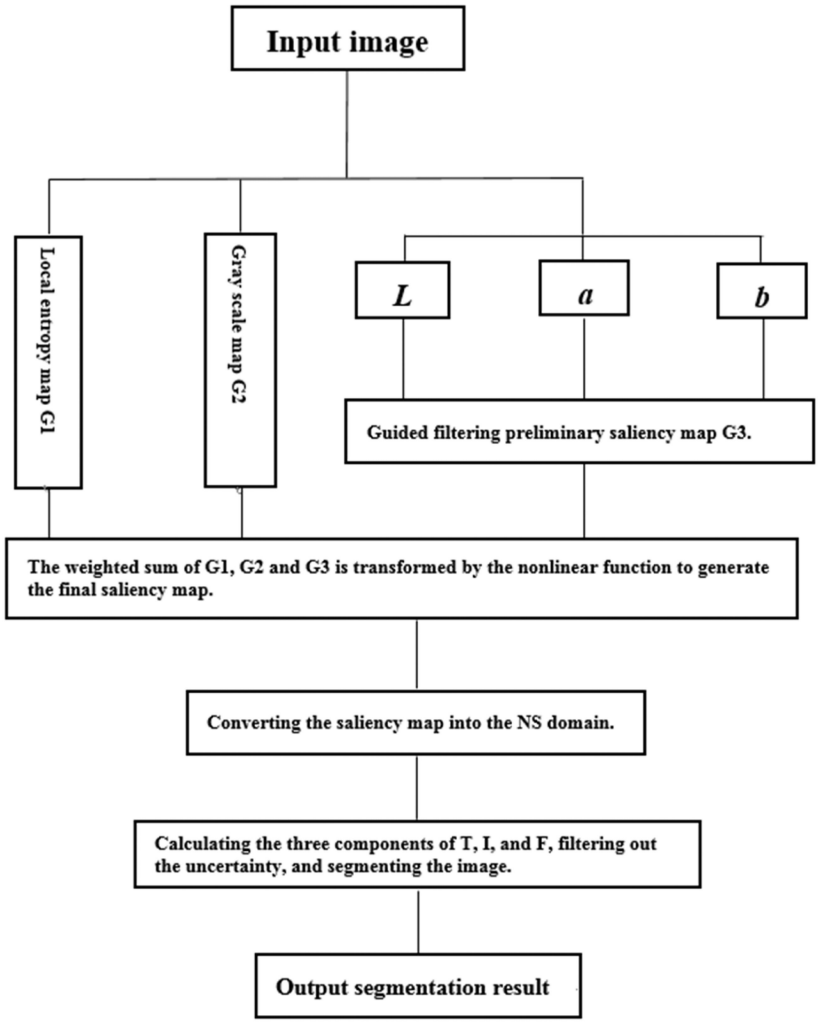

Fig. 1. The flowchart of the proposed algorithm.

is, the more pixels the image contains; the more uniform the grayscale distribution is, the more information the image contains, and vice versa.

In the image G, $G(x, y)$ is the gray value of the pixel at (x, y), the value of x is within the width W of the image G, and the value of y is within the length H of the image G, G (x, y) $\in$ {0, 1, …, L-1}, where L represents the maximum gray value of the image.

$$H_E = -\sum_{k=0}^{L-1} p_k * log_2 p_k \tag{1}$$

where $p_k = n_k/(W + H)$ represents the probability of the gray value k.

Only the local entropy needs to be calculated in the same way as the previous entropy value in each pixel and its neighborhood. Then, the neighborhood R of the pixel (x, y) is of size a$*$b, and the entropy expression for the range is as follows:

$$H_E(R) = -\sum_{t=0}^{L-1} p_t * log_2 p_t \tag{2}$$

where $p_t = n_t/(a+b)$ denotes the probability that the gray value t appears in the range of the neighborhood R, and n_t represents the number of gray values in the range of the neighborhood R. A local entropy map of the image G can be constructed using Eq.(2).

2.1.2 Guided Filter

The guided filter requires a guidance picture that can be a separate image or an input image. When the guidance picture is an input image, the guided filter becomes a filtering operation that maintains the edge. We adopt the input image as the guidance image in this paper.

In paper [12], the key assumption of the guided filter is a local linear model between the guidance I and the filter output q. The output formula of the guided filter is as follows:

$$q_i = a_k\, I_i + \ b_{k,} \forall\ i\ \in \omega_k \tag{3}$$

where (a_k, b_k) are some linear coefficients assumed to be constant in a window ω_k centered at the pixel k. And the radius of the window is r. This local linear model ensures that q has an edge only if I has an edge, since $\nabla q = a * \nabla I$.

To solve the coefficients a_k and b_k in (3), assume that p is the result before q filtering, and it satisfies the minimum difference between q and p. Then, it is transformed into the optimization problem, and the cost function is as follows:

$$E\,(a_k, b_k) = \sum_{i\in\omega_k} \left((a_k I_i + b_k - p_i)^2 + \ \epsilon a_k^2 \right) \tag{4}$$

where ϵ is a regularization parameter, that prevents the occurrence of a too large value.

$$a_k = \frac{\frac{1}{|\omega|}\sum_{i\in\omega_k} I_i p_i - \mu_k \bar{p}_k}{\sigma_k^2 + \varepsilon} \tag{5}$$

$$b_k = \bar{p}_k\ - a_k \mu_k \tag{6}$$

where μ_k and σ_k^2 respectively denote mean and variance of I in ω_k, $\bar{p}_k = \frac{1}{|\omega|}\ \sum_{i\in\omega_k} p_i$ is the mean of p in ω_k, and the number of pixels in ω_k is represented by $|\omega|$.

$$q_i = \frac{1}{|\omega|} \sum_{k:i\in\omega_k} (a_k I_i + b_k)\ \ = \bar{a}_i I_i + \ \bar{b}_i \tag{7}$$

where $\bar{a}_i = \frac{1}{|\omega|}\ \sum_{k\in\omega_i} a_k$, and $\bar{b}_i = \frac{1}{|\omega|}\ \sum_{k\in\omega_i} b_k$.

From (7), there is a linear relationship between the guidance image I and output q, such that the information provided by the guidance image can be used to indicate the edges. If the guidance image tells us that it is an edge, the final result tries to preserve the edge information.

After the guided filtering, according to the definition of paper [9], a preliminary saliency processing is started as follows:

$$S\,(x, y) = \ \ \left|\left| I\,(u) - I_q\,(x, y) \right|\right| \tag{8}$$

where $I(u)$ is the mean of the pixel value in image q, and $I_q(x, y)$ is the value at (x, y).

2.1.3 Nonlinear Function

The nonlinear function used in this paper is the sigmoid function, which is a mathematical function with a graceful sigmoid curve. It has a wide range of applications in logistic regressions and artificial neural networks. The mathematical form of the sigmoid function is as follows:

$$(x) = \frac{1}{1 + e^{-x}} \tag{9}$$

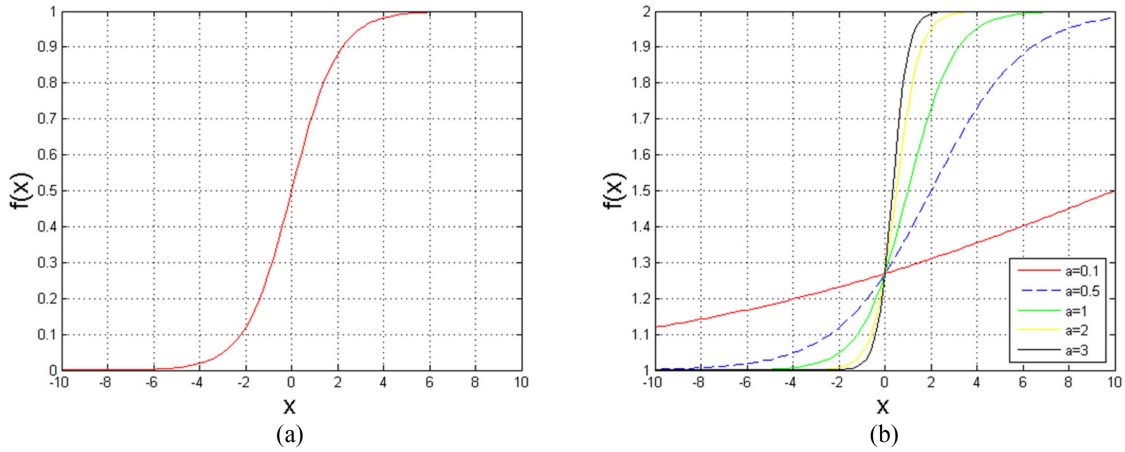

Fig. 2. (a) sigmoid function, and (b) redefined sigmoid function.

As seen from Fig. 2(a), the sigmoid function is continuous, smooth, strictly monotonous, and symmetric with a center of (0, 0.5), which is a very good threshold function. When x approaches negative infinity, y approaches 0; when x approaches positive infinity, y approaches 1; and when x = 0, y = 0.5.

It can be found that the output information of the image can be controlled by adjusting the zero point and the slope of the sigmoid function curve. Therefore, in this paper, an improved kind of function is redefined as follows:

$$f\ (x) = \frac{1}{1 + e^{-(ax-b)}} + m \tag{10}$$

Eq.(10) is the nonlinear function used in the paper, which add parameters *a*, *b*, and *m*, where *a* and *b* are used to control the sigmoid function curve radians and m is the vertical translation of the function values.

For example, $a = 0.1$, 0.5, 1, 2, and 3; $b = 1$; and $m = 1$. The curve is shown in Fig. 2(b). The slope changes when parameter *a* changes, and the slope increases as *a* increases. From the curve of $a = 1$ and $b = 1$, it is found that the zero point decreases, the two intervals are no longer symmetric, and *m* is used to adjust the value of the function. This allows you to control the slope and zero point by adjusting *a* and *b* to differently enhance and weaken the image to produce a saliency map. The process of saliency map generation is shown in Fig. 3.

2.2 Neutrosophic Set Theory

Neutrosophy analyzes and explores the indeterminacy in natural sciences and social sciences from the perspective of the unity of opposites. Its basic view is that all propositions and things have true, indeterminacy and false. If there is a proposition <A>, the opposite of <A> is <Anti-A>, neutrality <Neut-A> is neither <A> nor <Anti-A>, and the three neutrosophy memberships true, false, and indeterminate are used to represent the set of <A>, <Anti-A>, and <Neut-A> respectively. This logic has changed the traditional thinking of only true or false, and can better express the actual proposition of ambiguity and uncertainty; therefore, it is more in line with people's perception of things, propositions, concepts, etc. [23].

An image transformed to the NS domain consists of three subsets: true, indeterminate, and false. In a traditional set, $T = 0 (F = 1)$ or $T = 1 (F = 0)$; in the fuzzy set, $I = 0$, and the values of elements in T and F are [0, 1]; and in the neutrosophic set, the values of the elements in T, I and F are all [0, 1]. Thus, NS = {*T*(*i, j*), *I*(*i, j*), *F*(*i, j*)},and *T*, *I* and *F* can be calculated by the following equations [24],

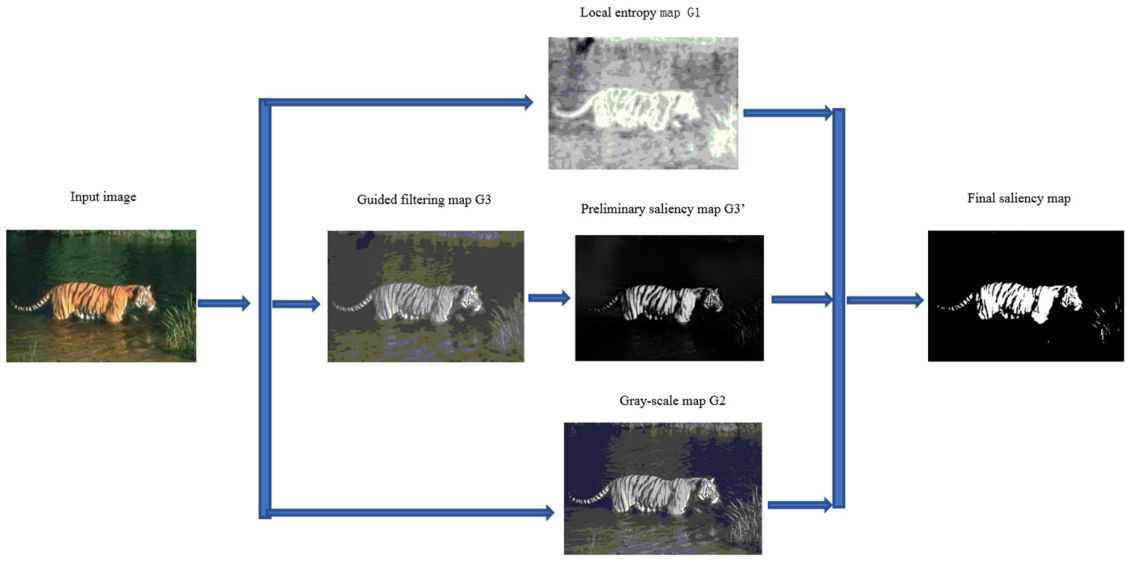

Fig. 3. The process of saliency map generation.

[30]:

$$T\ (i,\ j) = \frac{\bar{g}\,(i,\ j) - \bar{g}_{min}}{\bar{g}_{max} - \bar{g}_{min}} \tag{11}$$

$$\bar{g}\ (i,\ j) = \frac{1}{(2\omega+1)\times(2\omega+1)} \sum_{m\,=\,i-w}^{i+w} \sum_{n\,=\,j-w}^{j+w} g\,(m,\ n) \tag{12}$$

$$I\ (i,\ j) = \frac{\delta\,(i,\ j) - \delta_{min}}{\delta_{max} - \delta_{min}} \tag{13}$$

$$\delta\ (i,\ j) = \left|g\,(i,\ j) - \bar{g}\,(i,\ j)\right| \tag{14}$$

$$F\ (i,\ j) = \frac{\bar{g}_{max} - \bar{g}\,(i,\ j)}{\bar{g}_{max} - \bar{g}_{min}} \tag{15}$$

In (11-15), $g(i,\ j)$ denotes the input image, and $\bar{g}(i,\ j)$ is the local mean of $g(i,\ j)$ at $(i,\ j)$. $\delta(i,\ j)$ is the absolute value of the difference between the intensity $g(i,\ j)$ and its local mean value $\bar{g}(i,\ j)$. $\bar{g}_{max}$, $\bar{g}_{min}$ andδ_{max}, δ_{min} are the maximum and minimum values of $\bar{g}(i,\ j)$ and $\delta(i,\ j)$ respectively.

To fuse the three subsets of T, I and F together, the new entropy formula [32] was selected in this paper, which is defined as follows:

The entropy of an image pixel $\alpha = <\alpha_1,\alpha_2,\ \alpha_3>$ is a function E: $\Omega\rightarrow[0,1]$, which satisfies the following axiomatic requirements:

·$E\ (\alpha) =\ 0$ if and only if $\alpha_t =\ 0$ *or* $\alpha_t =\ 1,\ t\ =\ 0, 1, 2$;
·$E\ (\alpha) =\ 1$ if and only if $\alpha_t =\ 0.5,\ t\ =\ 0, 1, 2$;
·$E\ (\alpha) =\ E(\alpha^c)$; and
·$E(\alpha) \le E(\beta)$ if β more uncertain than α, i.e.,
$\alpha_t \le \beta_t$ when $\beta_t - {\beta_t}^c \le 0,\ t\ =\ 0, 1, 2,$

or
$\alpha_t \ge \beta_t$ when $\beta_t - {\beta_t}^c \ge 0,\ t\ =\ 0, 1, 2.$

Based on the cosine function, an information measure formula for an NS image is constructed as follows:

$$E\ (\alpha) = \frac{1}{3\left(\sqrt{2}-1\right)} \sum_{t=1}^{3} \left(\sqrt{2}cos\frac{\alpha_t - {\alpha_t}^c}{4}\pi - 1\right) \tag{16}$$

where α_1,α_2, and α_3 represent the three memberships *T*, *I*, and *F* respectively.

To decrease the indeterminacy again in the NS domain, a similarity measure method is employed to process the NS image. The similarity measure [32] is defined as follows:

Suppose that α and β are two pixels or regions. The similarity measure between α and β, which is denoted as $S\ (\alpha,\ \beta)$, should satisfy the following axiomatic requirements:

· $S(\alpha, \beta) = 0$, if and only if $\alpha_t = 0$ *or* $\alpha_t = 1,\ t = 0, 1, 2$;
· $S(\alpha, \beta) = 1$, if and only if $<\alpha_1, \alpha_2, \alpha_3> = <\beta_1, \beta_2, \beta_3>$;
· $S(\alpha, \beta) = S(\beta, \alpha)$;
·$S(\alpha, \gamma) \leq S(\alpha, \beta)$,$S(\alpha, \gamma) \leq S(\beta, \gamma)$, if $\alpha_t \leq \beta_t \leq \gamma_t$ or $\alpha_t \geq \beta_t \geq \gamma_t$, $t = 0, 1, 2$.

Based on the cosine function, an information measure formula for α and β is established as follows:

$$S\ (\alpha, \beta)\ = \frac{1}{3\left(\sqrt{2}-1\right)} \sum_{t=1}^{3} \left(\sqrt{2}cos\frac{\alpha_t - \beta_t}{4}\pi - 1\right) \tag{17}$$

where α_1, α_2, and α_3 represent the three memberships *T*, *I*, and *F* of α respectively, and the same is true for β_1, β_2, and β_3. If the value of $S(\alpha, \beta)$ exceeds 0.7, α and β will be merged into one class.

The previous work extends the similarity measure from only the partial similarity of *T* to the similarity of the three parts of *T*, *I* and *F*, which can achieve the purpose of improving the accuracy. Finally, we will provide clear saliency map, and then the Ostu threshold is used to segment it to get the final result.

3. Experiment and Results

In this section, we proved the effectiveness of the proposed algorithm by comparing the different algorithm segmentation results, the objective evaluation criteria, and the running time. The proposed algorithm has the ability to suppress several main noises. The images used in the experiment were from the MSRA10K [33, 38] image library, which has 10,000 images. All the experimental parameters in this paper are set as follows: the parameters of the guided filtering *r* and ε are set to 16 and 0.01 respectively, the weights of *G1*, *G2* and *G3* are 0.1, 0.1, and 0.8 respectively; and *x*, *y* and *m* are 0.5, 0.2, and 1 respectively, in the nonlinear function (10). Subject to change, there will be a special explanation.

Taking Fig. 2 as an example, first, the original image is transformed into the local entropy figure G1, the image G3 after the guided filtering in the L∗a∗b space, and the grayscale image G2. Then, (8) is used to generate the saliency map G3' of figure G3. Finally, the weighted superposition of G1, G2 and G3' are transformed using (10) to obtain a final saliency map. It can be seen intuitively that the final segmentation result is better than the salient segmentation map in Fig. 3, because the degree of under-segmentation has decreased.

The final segmentation map and the segmentation map of the salient map are segmented by the Ostu threshold method in Fig. 4. Therefore, the former is superior to the latter, which proves the filtering effect of NS theory on the indeterminacy of the image.

3.1 Comparison With Other Methods

To prove the effectiveness of the method proposed in this paper, we compare the SMNS model with the Saliency Driven Region-Edge-based Top Down Level Set Evolution Reveals the Asynchronous

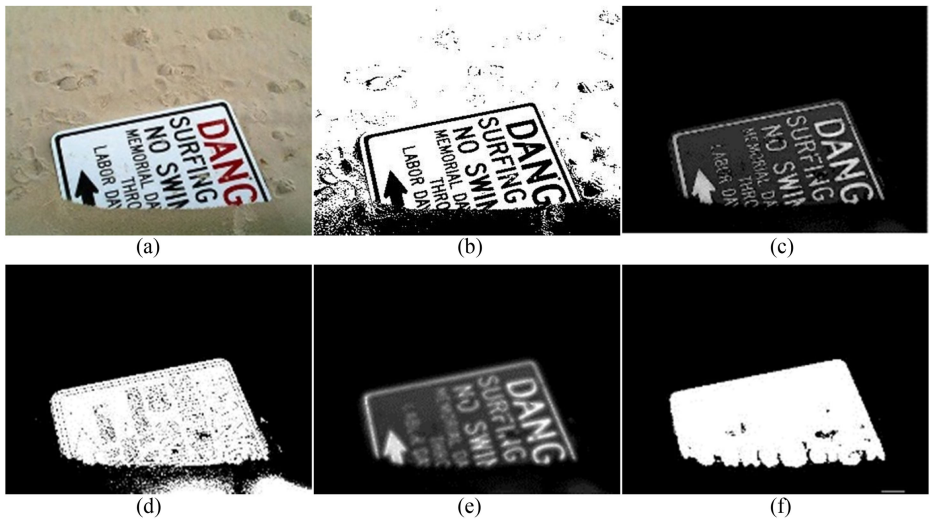

Fig. 4. (a) Original color image, (b) The Ostu segmentation result of (a), (c) The saliency map, (d) The Ostu segmentation result of (c), (e) The NS image, and (f) The Ostu segmentation result of (e) or the final segmentation result.

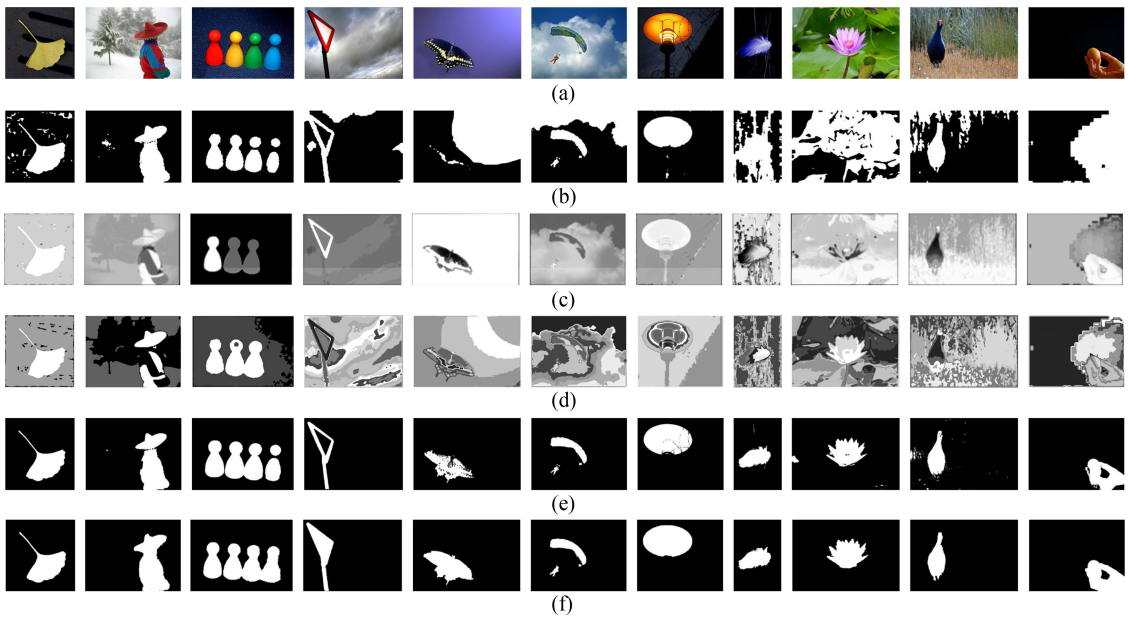

Fig. 5. (a) Original image, (b) Segmentation results of the SDREL model, (c) Segmentation results of the NMS model, (d) Segmentation results of the NCF model, (e) Segmentation results of the SMNS model, and (f) ground truth.

Focus in Image Segmentation (SDREL) [14]. An effective color image segmentation approach is applied that use neutrosophic adaptive mean shift clustering (NAMS) [31] and a novel image segmentation approach based on neutrosophic c-means clustering and indeterminacy filtering (NCF) [30]. In the SDREL model, a saliency map is generated, and then the level set model combined with the region information and the edge information is employed to quickly and accurately perform edge evolution and region segmentation, as shown in Fig. 5.b. The NAMS model consists of two parts. One part is the defined indeterminacy filter, which reduces the indeterminacy degree of an image through the indeterminacy membership value and the neighboring features. In the other part,

TABLE 1
Performance Parameters Considered for Evaluation of the Proposed Method With the Other Considered Methods for Image Segmentation

Parameters	Formulations	Remark
PRI	$\mathrm{PRI} = \frac{a+b}{a+b+c+d}$	Describzs the consistency of the segmented image and its ground truth
GCE	$\mathrm{GCE}(S_1, S_2) = \frac{1}{n}\{\sum_i E(S_1, S_2, p_i), \sum_i E(S_2, S_1, p_i),\}$	Measures the refinement in one segmentation over the other.
VoI	$\mathrm{VoI} = \mathrm{H}(S_1) + \mathrm{H}(S_2) - 2I(S_1, S_2)$	Determines the randomness in one segmentation from given segmentation in terms of distance.
Precision	$\mathrm{Precision} = \frac{N(Obj_{EX} \cap Obj_{GT})}{NObj_{EX}}$	The fraction of relevant pixels among the retrieved pixels.
Recall	$\mathrm{Recall} = \frac{N(Obj_{EX} \cap Obj_{GT})}{NObj_{GT}}$	The fraction of relevant pixels that have been retrieved over the total amount of relevant pixels.

mean shift clustering is applied to image segmentation, and its bandwidth is adaptively determined by the image's indeterminacy values. Its result is shown in Fig. 5.c. In the NCF model, a new filter is designed based on the indeterminacy membership value of the neutrosophic image, namely, the indeterminacy filter, which uses spatial information to eliminate the indeterminacy of spatial features. The indeterminacy filter is utilized to remove the indeterminacy in the intensity of the image. The parameters are determined by the results of neutrosophic c-means clustering, which has the advantage of describing the indeterminacy in the intensity, as shown in Fig. 5.d. The SMNS model proposed in this paper mainly includes two aspects. One is the saliency map and the other is the NS domain segmentation. First, we reconstruct a new saliency map based on the saliency map of equation (8), which is different from the saliency map in paper [14]. From Fig. 3, we can see that the saliency map of this paper is obviously and clearly separated from the background. After constructing the saliency map, NS theory is used to convert it to the NS domain, reduce the indeterminacy in it by measuring the similarity, and separate the target from the background. Then the Ostu threshold is employed to divide the image, and get a good segmentation result. In Fig. 4, we can clearly see the quality of the segmentation results of salient segmentation map and the final segmentation image. The research mentioned above converts the original image to the NS domain, while the NS domain in this paper addresses the saliency map. Therefore, the main purpose is to filter out the details in the saliency map that are not the target, to make the segmentation target clearer and better. As shown in Fig. 5.e, the segmentation result is closer to ground truth, which was in Fig. 5.f. Fig. 5 shows some visual examples where our result is superior to other algorithms.

For an objective assessment, five image segmentation performance parameters are used in Table 1 along with their formulations: the Probability Rand Index (PRI) [34], the Global Consistency Error (GCE) [35], the Variation of Information (VoI) [36], Precision and Recall [37], [38].

The objective performance of the proposed method is done using the five evaluation parameters presented in Table 1. Table 2 and Fig. 6 show the average values of each considered parameter on 10000 images from MSRA10K for image segmentation. From TABLE 2, it is observed that the maximum values of the PRI and Precision and the minimum value of the VoI are obtained by the proposed SMNS model, which illustrates the best segmentation consistency, accuracy and deviation. However, for the GCE and Recall parameters, the SDREL model and the NSM model have the most competitive results, respectively. Therefore, it is demonstrated that the proposed SMNS model has a better performance than other methods. The advantage of the SMNS model is obvious in Fig. 5, but the objective performance advantage in TABLE 2 is not significant. Because only a few excellent segmentation results are shown in Fig. 5, and the values in TABLE 2 are the average values of objective evaluation parameters on 10,000 images obtained from MSRA10K.

TABLE 2
Performance Comparison of the Proposed Method With the Other Considered Methods for MSRA10K

Parameters	SDREL	NSM	NCF	SMNS
PRI	0.726	0.674	0.662	0.736
GCE	0.168	0.176	0.187	0.173
VoI	1.019	1.050	1.520	0.964
Precision	0.590	0.472	0.656	0.679
Recall	0.695	0.762	0.606	0.680

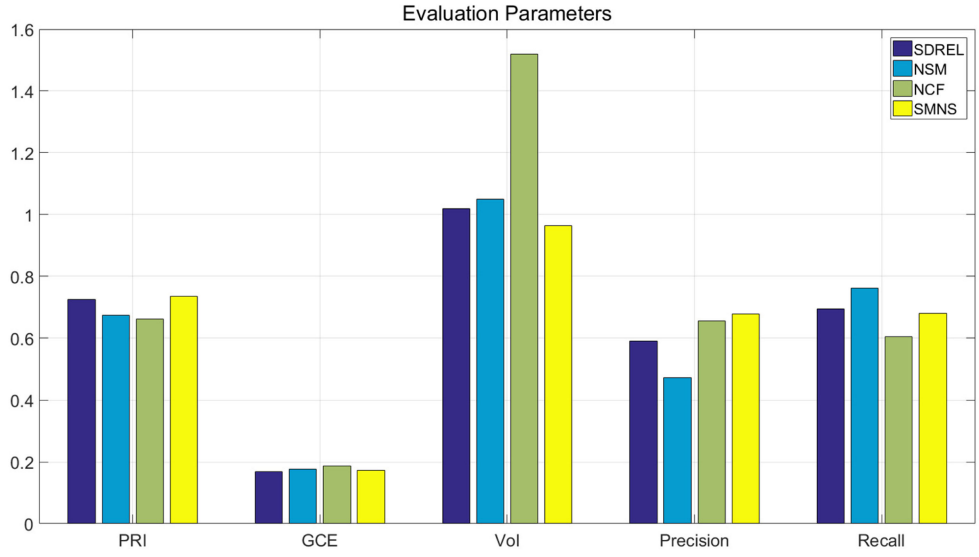

Fig. 6. Objective comparison of segmentation results on MSRA10K.

3.2 The Ability of De-Noising

To test and verify the effectiveness of the de-noising in this paper, Gaussian white noise was added artificially in Fig. 7 and Fig. 8, salt and pepper noise was appended in Fig. 9 and Fig. 10, and the above two mixed noises were added in Fig. 11. In Fig. 7, the parameter of the guided filter is set to $\varepsilon = 0.01$, and when the mean and variance of the Gaussian white noise are 0, 0.05 and 0.4, 0.01 respectively, the image segmentation result begins to deteriorate. In Fig. 8, the parameter of the guided filter is set to $\varepsilon = 0.1$, and when the mean and variance of Gaussian white noise are 0, 0.1 and 0.5, 0.01 respectively, the image segmentation results take worsens. In Fig. 9, when the parameter of the guided filter is set to $\varepsilon = 0.01$ and the density of the salt and pepper noise is 0.1, the effect of image segmentation starts deteriorating. In Fig. 10, when the parameter of the guided filter is set to $\varepsilon = 0.1$, and when the density of the salt and pepper noise is 0.2, the effect of image segmentation worsens. Meanwhile, in Fig. 11, where $\varepsilon = 0.1$, when the mean and variance of Gaussian white noise are 0.4 and 0.01, respectively, and the density of the salt and pepper noise is 0.05; and when the mean and variance of the Gaussian white noise are 0.1 and 0.05, respectively, and the density of the salt and pepper noise is 0.08; the image segmentation result worsens. This shows that both the NS domain and the guided filter, which can achieve better

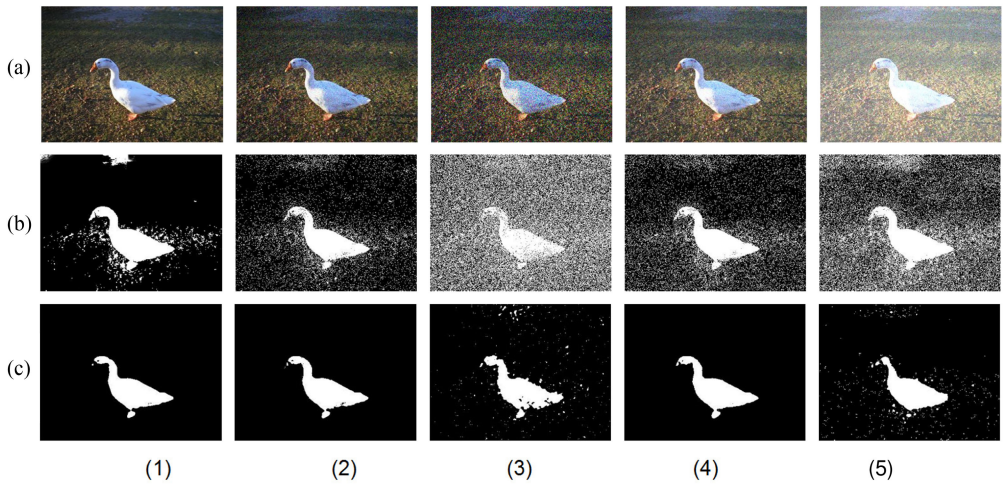

Fig. 7. (a) Original image, (b) Saliency map, and (c) Segmentation result of the SMNS. (1) The mean and variance of Gaussian white noise are set to 0 and 0 respectively, (2) The mean and variance of Gaussian white noise are set to 0 and 0.01 respectively, (3) The mean and variance of Gaussian white noise are set to 0 and 0.05 respectively, (4) The mean and variance of Gaussian white noise are set to 0.1 and 0.01 respectively, and (5) The mean and variance of Gaussian white noise are set to 0.4 and 0.01 respectively.

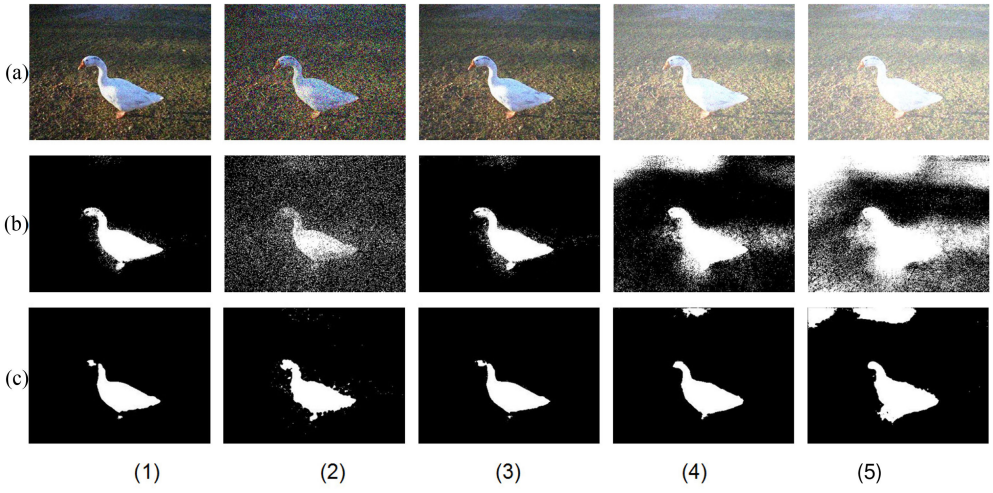

Fig. 8. (a) Original image, (b) Saliency map, and (c) Segmentation result of the SMNS. (1) The mean and variance of Gaussian white noise are set to 0 and 0.01 respectively, (2) The mean and variance of Gaussian white noise are set to 0 and 0.1 respectively, (3) The mean and variance of Gaussian white noise are set to 0.1 and 0.01 respectively, (4) The mean and variance of Gaussian white noise are set to 0.4 and 0.01 respectively, and (5) The mean and variance of Gaussian white noise are set to 0.5 and 0.01 respectively.

de-noising performance by adjusting the parameters, have the ability to remove Gaussian white noise, salt and pepper noise and their mixed noises.

3.3 Comparison of Running Time

All experiments are performed on a workstation with an Intel Core (TM) i5-6500 3.2GHz CPU and 4G memory using MATLAB. Compared with other aspects, the SMNS algorithm proposed in this paper has a significant advantage in the running time, as shown in Fig. 12. The average processing time of a single image is 0.35 seconds in the SMNS model, which is approximately seventeen

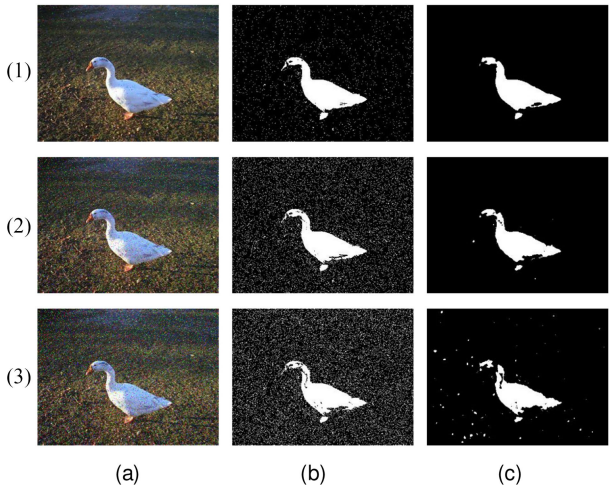

Fig. 9. (a) Original image, (b) Saliency map, and (c) Segmentation result of the SMNS. (1) The density of salt and pepper noise is set to 0.01, (2) The density of salt and pepper noise is set to 0.05, and (3) The density of salt and pepper noise is set to 0.1.

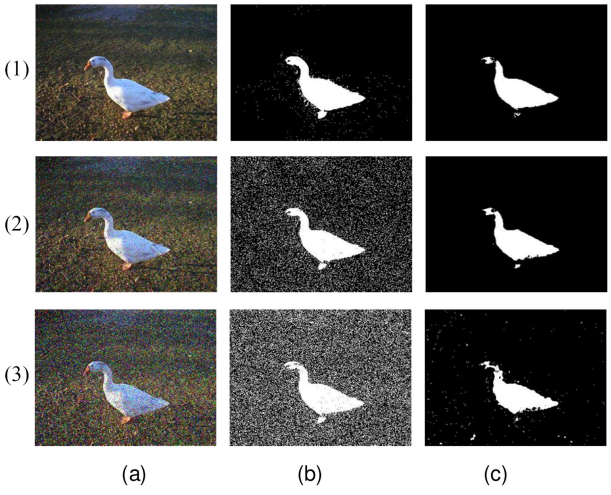

Fig. 10. (a) Original image, (b) Saliency map, and (c) Segmentation result of the SMNS. (1) The density of salt and pepper noise is set to 0.01, (2) The density of salt and pepper noise is set to 0.1, and (3) The density of salt and pepper noise is set to 0.2.

times faster than the 5.85 seconds of the NCF algorithm and more than five times faster than the 1.76 seconds of the SDREL method. There are two main reasons. One is that the comparison algorithms are level sets, mean shift and K-means algorithms, which have high time complexity. The other is that the time complexity of the SMNS algorithm is relatively low, which can be seen from the structure of this paper. Therefore, the SMNS algorithm has better real-time performance in image processing compared with the other considered methods.

4. Conclusion

A fast image segmentation algorithm combining the saliency map with NS theory is proposed to obtain a more accurate image segmentation. A series of experiments demonstrate the validity of our proposed algorithm, that is, the combination of the saliency map algorithm and NS theory can overcome their defects of under-segmentation and over-segmentation. Moreover, the SMNS model has a robust ability of de-noising to obtain better segmentation results of noise image,

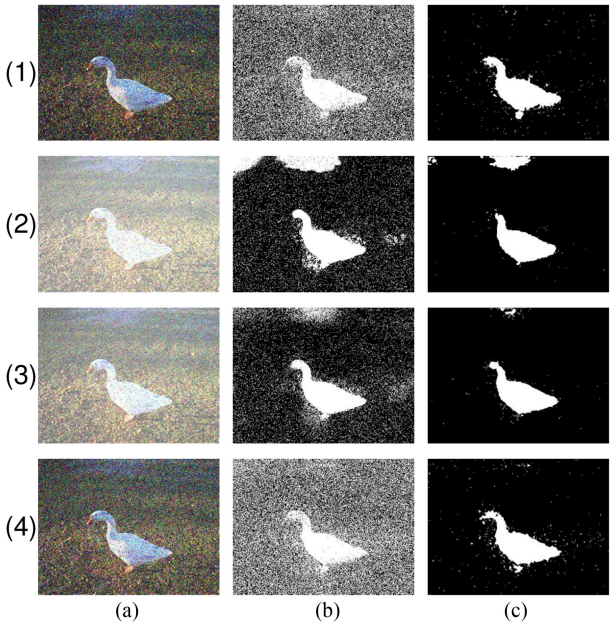

Fig. 11. (a) Original image, (b) Saliency map, and (c) Segmentation result of the SMNS. (1) The mean and variance of Gaussian white noise are set to 0 and 0.05 respectively, and the density of salt and pepper noise is 0.1, (2) The mean and variance of Gaussian white noise are set to 0.5 and 0 respectively, and the density of salt and pepper noise is 0.05, (3) The mean and variance of Gaussian white noise are set to 0.4 and 0.01 respectively, and the density of salt and pepper noise is 0.05, and (4) The mean and variance of Gaussian white noise are set to 0.1 and 0.05 respectively, and the density of salt and pepper noise is 0.08.

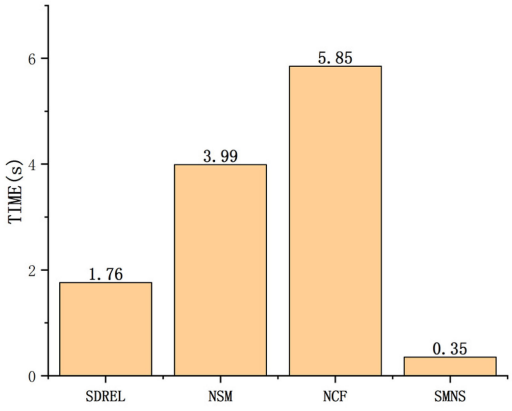

Fig. 12. The average running time of a single image on MSRA10K.

especially for Gaussian white noise, salt and pepper noise, and their mixed noise. Furthermore, most importantly, the prominent advantage of the SMNS model is very fast, which can improve the efficiency of large-scale image data processing. Although the SMNS model is considerably fast and has a powerful de-noising ability of image, the advantage of objective performance is limited. Therefore, the adjustment of algorithm structure and optimization of parameter settings will be explored to improve the objective performance of the SMNS model in future work.

References

[1] S. E. Palmer, "Vision science: Photons to phenomenology," *Quart. Rev. Biol.*, vol. 77, pp. 233–234, 1999.
[2] J. Shi, Q. Yan, L. Xu, and J. Jia, "Hierarchical image saliency detection on extended CSSD," *IEEE Trans. Pattern Anal. Mach. Intell.*, vol. 38, no. 1, pp. 717–729, Apr. 2016.
[3] L. Itti, C. Koch, and E. Niebur, "A model of saliency-based visual attention for rapid scene analysis," *IEEE Comput. Soc.*, vol. 20, no. 11, pp. 1254–1259, Nov. 1998.
[4] W. Zou, Z. Liu, K. Kpalma, J. Ronsin, Y. Zhao, and N. Komodakis, "Unsupervised joint salient region detection and object segmentation," *IEEE Trans. Image Process.*, vol. 24, no. 11, pp. 3858–3873, Nov. 2015.
[5] D. A. Klein and S. Frintrop, "Center-surround divergence of feature statistics for salient object detection," in *Proc. IEEE Int. Conf. Comput. Vis.*, 2011, pp. 2214–2219.
[6] M. M. Cheng, G. X. Zhang, N. J. Mitra, X. Huang, and S. M. Hu, "Global contrast based salient region detection," in *Proc. Comput. Vis. Pattern Recognit.*, 2011, pp. 409–416.
[7] Y. Fang, Z. Chen, W. Lin, and C.-W. Lin, "Saliency detection in the compressed domain for adaptive image retargeting," *IEEE Trans. Image Process.*, vol. 21, no. 9, pp. 3888–3901, Sep. 2012.
[8] F. Perazzi, P. Krähenbühl, Y. Pritch, and A. Hornung, "Saliency filters: Contrast based filtering for salient region detection," in *Proc. Comput. Vis. Pattern Recognit.*, 2012, pp. 733–740.
[9] R. Achanta, S. Hemami, F. Estrada, and S. Susstrunk, "Frequency-tuned salient region detection," in *Proc. Comput. Vis. Pattern Recognit.. IEEE Conf.*, 2009, pp. 1597–1604.
[10] C. Guo and L. Zhang, "A novel multiresolution spatiotemporal saliency detection model and its applications in image and video compression," *IEEE Trans. Image. Process.*, vol. 19, no. 1, pp. 185–198, Jan. 2010.
[11] J. Chen, B. Guan, H. Wang, X. Zhang, Y. Tang, and W. Hu, "Image thresholding segmentation based on two dimensional histogram using gray level and local entropy information," *IEEE Access*, vol. 6, pp. 5269–5275, 2018.
[12] K. He, J. Sun, and X. Tang, "Guided Image filtering," *IEEE Trans. Pattern Anal. Mach. Intell.*, vol. 35, no. 06, pp. 1397–1409, Jun. 2013.
[13] H. Fu, X. Cao, and Z. Tu, "Cluster-based co-saliency detection," *IEEE Trans. Image Process.*, vol. 22, no. 10, pp. 3766–3778, Oct. 2013.
[14] X. H. Zhi and H. B. Shen, "Saliency driven region-edge-based top down level set evolution reveals the asynchronous focus in image segmentation," *Pattern Recognit.*, vol. 80, pp. 241–255, 2018.
[15] H. Bi, H. Tang, G. Yang, H. Shu, and J. L. Dillenseger, "Accurate image segmentation using Gaussian mixture model with saliency map," *Pattern Anal. Appl.*, vol. 21, no. 3, pp. 869–878, 2018.
[16] L. Huo, L. Jiao, S. Wang, and S. Yang, "Object-level saliency detection with color attributes," *Pattern Recognit.*, vol. 49, pp. 162–173, 2016.
[17] S. Goferman, L. Zelnikmanor, and A. Tal, "Context-aware saliency detection," *IEEE Trans. Pattern Anal. Mach. Intell.*, vol. 34, pp. 1915–1926, Oct. 2012.
[18] N. Tong, H. Lu, Y. Zhang, and R. Xiang, "Salient object detection via global and local cues," *Pattern Recognit.*, vol. 48, pp. 3258–3267, 2015.
[19] C. Gong *et al.*, "Saliency propagation from simple to difficult," in *Proc. IEEE Conf. Comput. Vision Pattern Recognition*, Boston, MA, 2015, pp. 2531–2539, doi: 10.1109/CVPR.2015.7298868.
[20] Y. Xie, H. Lu, and M.-H. Yang, "Bayesian saliency via low and mid level cues," *IEEE Trans. Image Process.*, vol. 22, no. 5, pp. 1689–1698, May 2013.
[21] N. Liu and J. Han, "A deep spatial contextual long-term recurrent convolutional network for saliency detection," *IEEE Trans. Image Process. A Publication IEEE Signal Process. Soc.*, vol. 27, 2018, Art. no. 3264.
[22] L. Wang, H. Lu, X. Ruan, and M. H. Yang, "Deep networks for saliency detection via local estimation and global search," in *Proc. IEEE Conf. Comput. Vis. Pattern Recognit.*, 2015, pp. 3183–3192.
[23] F. Smarandache, "A unifying field in logics: Neutrosophic logic, neutrosophic set, neutrosophic probability and statistics (fourth edition)," in *Proc. Int. Conf. Neutrosophy, Neutrosophic Log., Neutrosophic Set, Neutrosophic Probability Statist.*, 2012, pp. 5–21.
[24] Y. Guo and H. D. Cheng, "New neutrosophic approach to image segmentation," *Pattern Recognition*, vol. 42, no. 5, pp. 587–595, May 2009.
[25] Y. Guo, "A novel image segmentation algorithm based on neutrosophic similarity clustering," *Appl. Soft Comput.*, vol. 25, pp. 391–398, Dec. 2014.
[26] A. Sengur and Y. Guo, "Color texture image segmentation based on neutrosophic set and wavelet transformation," *Comput. Vis. Image Understanding*, vol. 115, pp. 1134–1144, 2011.
[27] A. Heshmati, M. Gholami, and A. Rashno, "Scheme for unsupervised colour–texture image segmentation using neutrosophic set and non-subsampled contourlet transform," *Iet Image Process.*, vol. 10, pp. 464–473, 2016.
[28] Y. Guo, A. Şengür, and J. W. Tian, "A novel breast ultrasound image segmentation algorithm based on neutrosophic similarity score and level set," *Comput. Methods Programs Biomed.*, vol. 123, pp. 43–53, 2015.
[29] A. Rashno *et al.*, "Fully-automated segmentation of fluid/cyst regions in optical coherence tomography images with diabetic macular edema using neutrosophic sets and graph algorithms," *IEEE Trans. Biomed. Eng.*, vol. 65, no. 5, pp. 989–1001, May 2018.
[30] Y. Guo, R. Xia, A. Şengür, and K. Polat, "A novel image segmentation approach based on neutrosophic C-means clustering and indeterminacy filtering," *Neural Comput. Appl.*, vol. 28, no. 10, pp. 3009–3019, 2016.
[31] Y. Guo, A. Şengür, Y. Akbulut, and A. Shipley, "An effective color image segmentation approach using neutrosophic adaptive mean shift clustering," *Measurement*, vol. 119, pp. 28–40, 2018.
[32] H. Wu, Y. Yuan, L. Wei, and L. Pei, "On entropy, similarity measure and cross-entropy of single-valued neutrosophic sets and their application in multi-attribute decision making," *Soft Comput.*, vol. 22, no. 22, pp 7367–7376, 2018.
[33] M. Cheng, N. J. Mitra, X. Huang, P. H. S. Torr, and S. Hu, "Global contrast based salient region detection," *IEEE Trans. Pattern Anal. Mach. Intell.*, vol. 37, no. 3, pp. 569–582, Mar. 1, 2015.

[34] C. Pantofaru and M. Hebert, "A comparison of image segmentation algorithms," in *Proc. Biomed. Eng. Int. Conf.*, 2015, pp. 1–4.
[35] D. Martin, C. Fowlkes, D. Tal, and J. Malik, "A database of human segmented natural images and its application to evaluating segmentation algorithms and measuring ecological statistics," *Proc. 8 IEEE Int. Conf. Comput. Vis., ICCV*, 2001, Vancouver, BC, Canada, pp. 416–423, 2001.
[36] M. Meila, "Comparing clusterings: An axiomatic view," in *Proc. 22nd Int. Conf. Mach. Learn.*, 2005, pp. 577–584.
[37] D. Ren, Z. Jia, J. Yang, and N. K. Kasabov, "A Practical Grabcut color image segmentation based on bayes classification and simple linear iterative clustering," *IEEE Access*, vol. 5, pp. 18480–18487, 2017.
[38] A. Borji, M. M. Cheng, H. Jiang, and J. Li, "Salient object detection: A benchmark," *IEEE Trans. Image Process.*, vol. 24, no. 12, pp. 5706–5722, Dec. 2015.